ACS Sustainable Chemistry & Engineering

Research Article

pubs.acs.org/journal/ascecg

Ultratough, Ductile, Castor Oil-Based, Hyperbranched, Polyurethane Nanocomposite Using Functionalized Reduced Graphene Oxide

Suman Thakur and Niranjan Karak*

Advanced Polymer and Nanomaterial Laboratory, Department of Chemical Sciences, Tezpur University, Tezpur 784028, India

Supporting Information

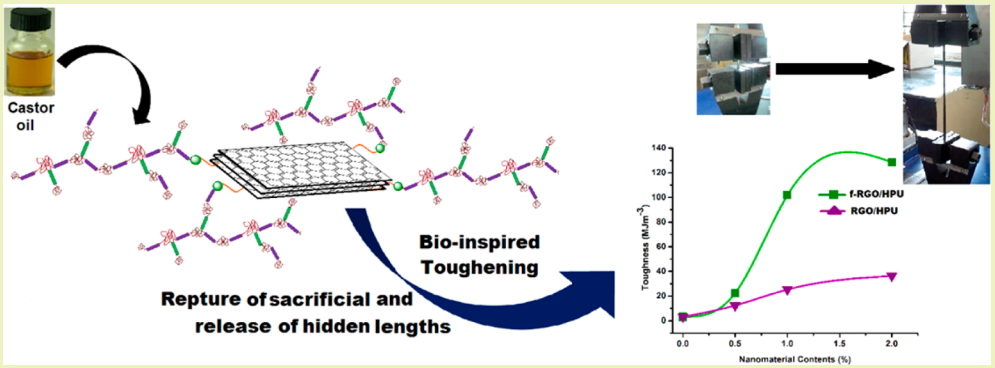

ABSTRACT: We reported on an ultratough, ductile, castor oil-based, hyperbranched, polyurethane (HPU) nanocomposite using functionalized reduced graphene oxide (f-RGO) as a reactive chain extender as well as a nano-reinforcing material. The functionalization of phytoextract-reduced graphene oxide (RGO) was achieved by reacting with 2,4/2,6-toluene diisocyanate, followed by reacting with 1,4-butanediol. Functionalization (hydroxyl group-terminated urethane linkage) in f-RGO was confirmed by FTIR and XRD studies. The obtained nanocomposite demonstrated tremendous enhancements of tensile strength (525%), modulus (42 folds), and toughness (18 folds) after incorporation of 2 wt % of f-RGO in HPU. Most surprisingly, elongation at break of the nanocomposites was enhanced from 710% to a maximum of 1656%. On other hand, the HPU nanocomposite with RGO was unable to demonstrate improved properties similar to those of HPU/f-RGO nanocomposites. The HPU/f-RGO nanocomposite also demonstrated good thermal stability and excellent electrical conductivity with an enhancement of almost 10 orders of magnitude at 2 wt % f-RGO. The effective and promising technique presented here paves the way to graphene-based polymer nanocomposites with excellent performance and novel functionalities.

KEYWORDS: *Hyperbranched, Reduced graphene oxide, Biobased, Ultratough, Conductive*

INTRODUCTION

Vegetable oil-based hyperbranched polyurethane is an important class of polymer because it is a renewable source available from the global community.[1−3] Renewable resources are important due to the decline of petroleum reserves, threat of global warming, and stringent environmental rules and regulations.[4,5] Among the various vegetable oils, castor oil is one of the best industrial choices. This is due to its unique composition of fatty acid and ease of availability.[6] Again, it is pertinent to mention here that such biobased hyperbranched polymers have garnered copious interest in recent years owing to the their functionality, three-dimensional unique structural architectures, low melt and solution viscosity, high reactivity, good compatibility with others. and so on.[7] All of these features have a profound influence on processing and the ultimate performance of such polymers. However, hyperbranched polyurethane also has a few inefficiences, such as poor mechanical properties including tensile modulus and low electrical conductivity that limit to address many *avant-garde* applications such as in actuators, photovoltaic cells, scaffolding, and so forth.[8] Although a recent approach of incorporation of a long segment in such hyperbranched polyurethanes resulted in improved mechanical performance, it was unable to reach the expectation of advanced applications.[9,10] In this milieu, nanotechnology has a great influence on improving many desired properties, including mechanical properties.

In this context, much attention has been paid to polymer nanocomposites with carbon nanomaterials because the incorporation of carbon nanomaterials can effectively enhance the thermal, mechanical, and electrical properties of the nanocomposites.[11−18] Among the genre of carbon-based nanomaterials, graphene has carved a distinctive niche of its own due to its high electron mobility, excellent thermal conductivity, excellent mechanical strength, large surface area, and high thermal stability.[19−34] The incorporation of graphene into a polymer matrix is one of the promising ways to harness the

Received: January 13, 2014
Revised: March 28, 2014
Published: April 8, 2014

mechanical and electrical properties of the pristine polymer for its above advance applications. However, homogeneous dispersion of graphene in the polymer matrix is a paramount factor as aggregation or restacking of graphene sheets commonly occurs in most of the cases because of the $\pi-\pi$ stacking and hydrophobic interactions among the sheets.[35] Again, the weak interactions between graphene and the polymeric matrix result in interfacial slippage on application of external stress, limiting the improvement of mechanical properties.[36]

Although functionalization is a promising way to improve dispersibility and interactivity of graphene with the polymer matrix, such functionalization of graphene is difficult due to its inertness.[37] On the other hand, graphene oxide (GO) and modified GO have good dispersibility and compatibility with polar polymers including polyurethane, which help in augmenting the desired mechanical performance of pristine polymers.[38] However, such nanocomposites are found to be insulating in character by incorporation of these electrically insulating nanomaterials.[39] Furthermore, reduced GO (RGO) can simultaneously improve the mechanical as well as electrical properties of pristine polyurethane.[40]

In this investigation, an effective technique is demonstrated to fabricate castor oil-based, highly tough, elastic hyperbranched polyurethane nanocomposites using functionalized reduced graphene oxide (f-RGO) as a reactive chain extender as well as reinforcing nanomaterial at different weight percentages. These *in situ* generated hyperbranched polyurethane/f-RGO nanocomposites are characterized by FTIR, XRD, DSC, and TGA. The performance, including mechanical and electrical properties of the nanocomposites, was also investigated.

EXPERIMENTAL SECTION

Materials. Glycerol (Merck, India), castor oil (Sigma-Aldrich), 1,4-butanediol (BD, Merck, Germany), and poly(ϵ-caprolactone) diol (PCL, Solvay Co., M_n= 3000 g mol^{-1}) were used after drying in an oven prior to use. Concentrated sulfuric acid (98%, Merck, India), hydrogen peroxide (H_2O_2, 30%, Merck, India), concentrated hydrochloric acid (30%, Merck, India), potassium permanganate ($KMnO_4$, Analytical Rasayan, India), graphite flakes (60 mesh, purity 99%, Loba Chemie, India), calcium oxide (CDH, India), and 2,4/2,6-toluene diisocyanate (TDI, Merck, Germany) were used as received. Xylene (Mecrk, India) and N,N-dimethylacetamide (Merck, India) were vacuum distilled and kept in 4A type molecular sieves before use. Other chemicals and solvents were of reagent grade and used without further purification. Monoglyceride of the castor oil was prepared as reported earlier.[6]

Preparation of RGO. GO was prepared by the modified Hummers method as reported earlier.[41] Oxidation of graphite powder was achieved by using a mixture of concentrated sulfuric acid and $KMnO_4$. Reduction of GO occurred at room temperature using aqueous phytoextract of *Colocasia esculenta* leaves as reported in our previous work.[41]

Functionalization of RGO. The amount of reactive hydroxyl group on RGO was 0.58 mmol/g as measured by a titrimetric method using butyl amine. The excess isocyanate was determined after reacting RGO with a known amount of TDI at 70 °C. On the basis of the above result, functionalization on RGO sheets was done by reacting with a required amount of TDI followed by BD. Briefly, 2 g of RGO was dispersed in 100 mL of distilled THF by overnight mechanical stirring followed by 15 min sonication. This dispersed RGO was taken in a three-necked round-bottomed flask equipped with a mechanical stirrer, nitrogen inlet, and Teflon septum. Then, 0.5 mmol of TDI was added dropwise into the reaction mixture at room temperature by help of a syringe through the septum. The reaction was continued for 4 h at a temperature of 70 ± 2 °C to obtain isocyanate terminated RGO. Then, 0.5 mmol of BD was dropwise added into the mixture, and the reaction was continued for another 1 h to obtain the desired f-RGO. This f-RGO was centrifuged and washed with THF to separate the free reactants. The f-RGO was dried in a vacuum oven at 45 °C overnight prior to use.

Preparation of Hyperbranched Polyurethane Using f-RGO as a Reactive Chain Extender. A three-necked round-bottomed flask equipped with a nitrogen gas inlet, mechanical stirrer, and Teflon septum was used for the polymerization reaction. Required amounts of PCL (0.002 mol, 6 g), BD (0.004 mol, 0.36 g), and dispersed f-RGO in DMAc (different wt %: 0.5, 1, and 2 with respect to total weight of nanocomposite) were taken in the reaction flask containing the desired amount of xylene with constant stirring (37% solid content). After dissolving the PCL, the desired amount of TDI (0.007 mol, 1.22 g) was added dropwise with a syringe into the reaction mixture at room temperature. The reaction was continued for 3 h at a temperature of 70 ± 2 °C to obtain the desired viscous mass, which was treated as the prepolymer.

This prepolymer was then cooled to room temperature, and a monoglyceride of castor oil (0.002 mol, 0.74 g) as a triol was added with the required amount of TDI (0.002 mol, 0.35 g). The temperature was then raised again to 110 ± 2 °C and stirred continuously for 2.5 h to complete the reaction, as indicated by the absence of an isocyanate band at 2270 cm^{-1} in the FTIR spectrum. This polymerization generates an *in situ* biobased, hyperbranched, polyurethane/f-RGO nanocomposite.

Following the same procedure, other sets of nanocomposites were also synthesized using different weight percentages of RGO. Hyperbranched polyurethane was also prepared without using f-RGO or RGO. Hyperbranched polyurethanes with 0.5, 1, and 2 wt % of f-RGO are encoded as HPU/f-RGO0.5, HPU/f-RGO1, and HPU/f-RGO2, respectively, and 0.5, 1, and 2 wt % of RGO are encoded as HPU/RGO0.5, HPU/RGO1, and HPU/RGO2, respectively. Hyperbranched polyurethane without f-RGO or RGO is coded as HPU.

Instruments and Testing Methods. The FTIR spectra of the polyurethanes were measured over the wavenumber range of 4000−400 cm^{-1} by a Nicolet (Madison, WI) FTIR impact 410 spectrophotometer using KBr pellets. The thermal analysis, TGA, was done by a Shimadzu thermal analyzer, TGA50, with a nitrogen flow rate of 30 mL/min at a heating rate of 10 °C/min, and the differential scanning calorimetry (DSC) was done by a DSC 60 (Shimadzu, Japan) at a 2 °C min^{-1} heating rate under a nitrogen flow rate of 30 mL min^{-1} from −20 to 120 °C. Scratch hardness of the dry film was measured by using a scratch tester, model number 705 (Sheen instrument Ltd., U.K.) with a stylus accessory and a travel speed of 30−40 mm/s. The fracture surface morphology of the nanocomposite was examined by a scanning electron microscope (JEOL, JSM-6390LV) after gold coating on the surface. The tensile strength and elongation at break were measured with a Universal Testing Machine (UTM), Jinan WDW 10 (China) with a 500 N load cell and crosshead speed of 20 mm/min. The X-ray diffraction study was carried out at room temperature (about 25 °C) by a Rigaku X-ray diffractometer (Miniflex, U.K.) with Cu Kα irradiation (λ = 0.154 nm) over a range of 2θ = 10−70° at a scan rate 2°/min. The impact strength was measured by an impact tester (S.C. Dey & Co., Kolkata; 100 cm is the maximum height) using the standard ASTM D-1037 falling weight method. A weight of 850 g was allowed to fall on the mild steel plate coated film from a minimum to maximum height up to which the film was not damaged. The maximum height was taken as the impact strength. Conductivities of the polymer films are measured as a function of frequency by using a Hioki-3532−50 LCR Hitester instrument. Sample films were loaded between the two circular electrodes (20 mm in diameter with 0.5 mm thickness) of the device and tested under ambient conditions.

RESULT AND DISCUSSIONS

Functionalization of RGO. The functionalization was achieved by reacting the isocyanate groups of TDI with the residual oxygenated functional groups of RGO sheets to obtain an isocyanate-terminated RGO sheet, followed by reacting with BD. Stable dispersion of f-RGO even after 2 months of storage in various solvents such as DMF, DMSO, THF, and DMAc was observed as shown in Figure S1 of the Supporting Information.

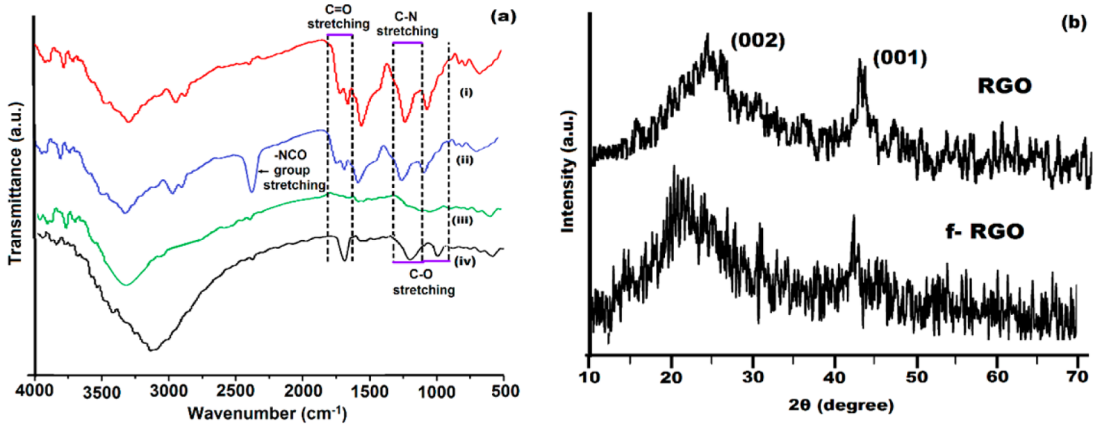

Figure 1. (a) FTIR spectra of (i) f-RGO, (ii) isocyanate-terminate RGO, (iii) RGO, and (iv) GO and (b) XRD patterns of f-RGO and RGO. [FTIR spectra of GO and RGO and XRD patterns of RGO are reproduced from our earlier work for better understanding[19]].

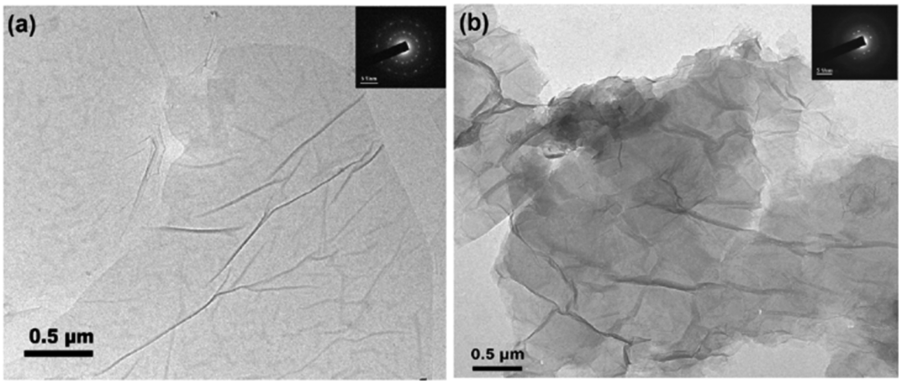

Figure 2. TEM images of (a) RGO and (b) f-RGO, and their SEAD patterns are shown in the inset.

FTIR spectra of GO, RGO, isocyanate-terminated RGO, and f-RGO are shown in Figure 1a. In the RGO spectrum, disappearance of the bands of C═O stretching, C−O−C stretching, and C−O stretching of the oxygen-containing groups of GO confirmed the removal such groups and reduction of GO.[41,42] The presence of urethane linkage in the FTIR spectrum of the intermediate (before adding BD) indicated the reaction of TDI with RGO. In the spectra of the intermediate product (isocyanate-terminated RGO) and f-RGO, two new bands appeared in the ranges of 2800−2880 and 2880−3000 cm^{-1}, which are assigned to the symmetric and asymmetric stretching vibrational bands of the $-CH_2$ groups,[1] resepctively. More direct evidence was obtained from the absorption at 1701, 1646, 1219, 1054, and 1543 cm^{-1} appearing in the spectra of both, which are attributed to the stretching vibration of carbonyl of amide I, C═C, C−O, C−N, and bending of N−H of amide II of urethane linkage, respectively.[6,9] This analysis indicates the validity of the covalent bond formation with RGO.

RGO shows a broad peak centered at $2\theta = 25°$, corresponding to *d*-spacing of 0.36 nm for the d_{002} plane in the XRD pattern (Figure 1b).[41] After functionalization of RGO, this peak was shifted to the lower angle (2θ = 21.2°, corresponding to *d*-spacing of 0.415 nm), which indicates that the *d*-spacing between the layers increased due to the presence of urethane chains.

TEM images of RGO and f-RGO are shown in Figure 2. More folds or wrinkles were found after the functionalization of RGO. The enhancement of the amorphous nature of RGO after functionalization was further confirmed by SAED patterns (inset of Figure 2).

HPU/f-RGO Nanocomposites. Castor oil-based, hyperbranched, polyurethane nanocomposites were obtained through covalent and noncovalent linkages of f-RGO with the prepolymer chains of HPU. Herein, f-RGO acts as a reactive chain extender in the prepolymerization step as well as nanoreinforcing material in the formation of nanocomposites. The covalent functionalization was achieved by direct linkage of a hydroxyl group of f-RGO and isocyanate groups. On the other hand, the noncovalent functionalization is attained by H-bonding between unreacted the hydroxyl group of f-RGO and urethane linkages of HPU as well as the $\pi-\pi$ conjugate interactions between pyrene rings of f-RGO and aromatic moiety of TDI unit.

FTIR spectra of HPU, HPU/RGO0.5, HPU/RGO1, and HPU/RGO2 are shown in Figure 3. The presence of characteristic bands at 1060−1090 (N−H deformation vibration), 1140−1175 (C−O stretching vibration), 1557−1580 (amide II: C−N stretching and N−H bending vibration), 1601−1635 (C═C stretching vibration), 1720−1730 (C═O stretching vibration, amide I), 2859−2950 (CH_2 symmetric and antisymmetric stretching vibrations), and 3430 cm^{-1} (O−H free and N−H stretching vibrations) clearly confirmed the formation of urethane linkage, −NH−C(═O)−O− in HPU (as reported in our earlier work[6]), and its nanocomposite.[8,43] The increase in broadening of the −OH band and shifting of the C═O band to 1690 from 1720 cm^{-1} was observed with an increasing amount of f-RGO in the nanocomposite. This confirmed the presence of interactions among the HPU chains and f-RGO, which were enhanced with the f-RGO content.

dx.doi.org/10.1021/sc500165d | ACS Sustainable Chem. Eng. 2014, 2, 1195−1202

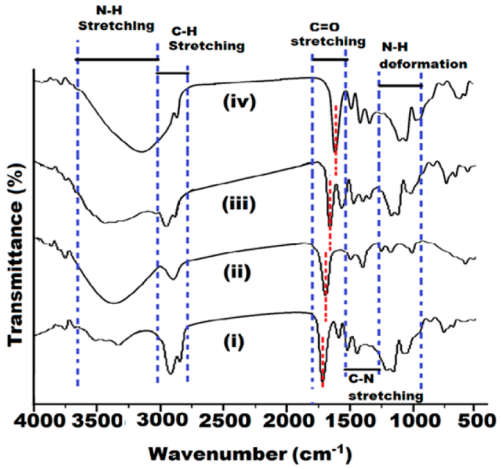

Figure 3. FTIR spectra of (i) HPU, (ii) HPU/f-RGO0.5, (iii) HPU/f-RGO1, and (iv) HPU/f-RGO2. [FTIR spectrum of HPU is reproduced from our earlier work for better understanding[6]].

The XRD patterns of HPU (reproduced from our earlier work[6]) and its nanocomposites showed two peaks at $2\theta = 21.1°$ (corresponding to d-spacing of 0.419 nm) and 23.4° (corresponding to d-spacing of 0.381 nm) for the crystals of PCL moiety of HPU (Figure 4).[6] Here, it is important to mention that no separate peak was observed for f-RGO in the nanocomposites. This may be due to the presence of a small amount of f-RGO in the nanocomposite. In the nanocomposites, PCL peaks were slightly shifted toward the higher angle owing to formation of the dense structure compared to the pristine HPU. Also, the peak intensity of the PCL moiety marginally increased with an increase in the amount of f-RGO due to the nucleating effect of f-RGO.

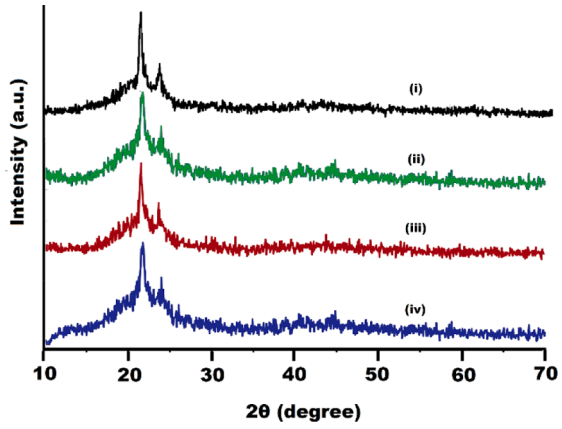

Figure 4. XRD patterns of (i) HPU, (ii) HPU/f-RGO0.5, (iii) HPU/f-RGO1, and (iv) HPU/f-RGO2. [XRD pattern of HPU is reproduced from our earlier work for better understanding[6]].

Figure 5 demonstrated the fracture morphology of the nanocomposite films. The nanocomposite exhibited a micro-rough fracture surface that can be attributed to the matrix shear yielding or the deformation of polymer between f-RGO.[44] The SEM micrograph showed that the structural deformation of the nanocomposite is aligned in the same direction.

Mechanical Properties. An extensive enhancement in the mechanical property of the *in situ* generated nanocomposites is due to the existence of covalent bonding between the rigid f-RGO and isocyanate-terminated prepolymer. This helps to form strong interfacial interactions between the polyurethane chain and homogeneously dispersed f-RGO. The values of tensile strength (σ), tensile modulus (E), toughness (T), and elongation at break (ε%) of HPU and HPU/f-RGO nanocomposites with different loadings of f-RGO are tabulated in Table 1, and the typical stress−strain profiles are shown in Figure 6. All the nanocomposites showed better mechanical properties compared to HPU (reproduced from our earlier work[6]). In addition to the above, a dose-dependent mechanical property of nanocomposites was noticed. Tensile modulus and toughness were enhanced enormously after the formation of the nanocomposite with 2 wt % of f-RGO. Also, HPU/f-RGO nanocomposites exhibited superior mechanical properties compared to the respective HPU/RGO nanocomposites. This confirmed the presence of stronger interactions with homogeneous distributions of f-RGO in HPU/f-RGO nanocomposites than with RGO in HPU/RGO nanocomposites.

Such superior mechanical properties can certainly be ascribed to the strong interfacial adhesion and good compatibility between f-RGO and the HPU matrix.[45,46] The hard domain of HPU is stiffened due to the presence of a strong covalent bond between f-RGO and HPU chains.[43] For this reason, the resulted nanocomposites exhibited unusual improvement in the tensile modulus (Figure 6). In addition to that, the high strength indicates preferential orientation of the rigid f-RGO in the matrix at high strains, and hence, synergistic effect was observed. This contributes to the dramatic enhancement of modulus.[47]

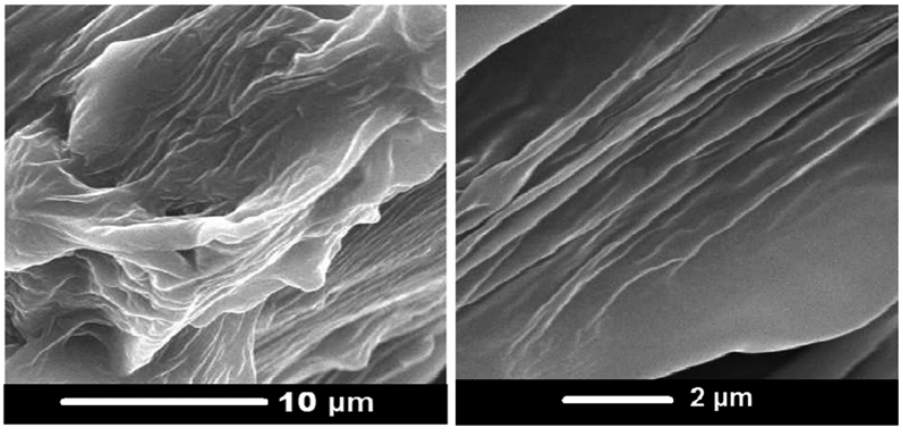

Figure 5. SEM micrographs of the fracture surface of HPU/f-RGO1.

Table 1. Mechanical Properties of HPU and Nanocomposite Films

sample	HPU[a]	HPU/f-RGO0.5	HPU/f-RGO1	HPU/f-RGO2	HPU/RGO0.5	HPU/RGO1	HPU/RGO2
σ^b (MPa)	7.16 ± 0.4	25.6 ± 1.3	33.4 ± 2.1	37.6 ± 1.8	17.6 ± 1.5	24.8 ± 1.6	27.8 ± 1.9
E^c(MPa)	3.09 ± 0.2	22.4 ± 0.4	101.8 ± 3.4	128.5 ± 4.2	12.4 ± 1.2	25.3 ± 1.1	36.3 ± 3.2
ε (%)	710 ± 35	1256 ± 50	1432 ± 32	1656 ± 43	890 ± 28	940 ± 46	980 ± 34
T (MJ/m^3)	25.40 ± 2.4	107.9 ± 4.3	348.16 ± 5.1	454.82 ± 6.2	63.72 ± 2.1	96.34 ± 3.4	115.78 ± 4.1
scratch hardness (kg)	5 ± 0.2	6.5 ± 0.1	7 ± 0.1	7.5 ± 0.1	5.5 ± 0.2	6 ± 0.2	6.5 ± 0.1
impact strength (cm)	>100	>100	>100	>100	>100	>100	>100

[a]Data of mechanical properties of HPU are reproduced from our earlier work for better understanding.[6] [b]Defined as the stress at the fracture point. [c]Obtained from the slopes of the elastic region in the stress−strain curves.

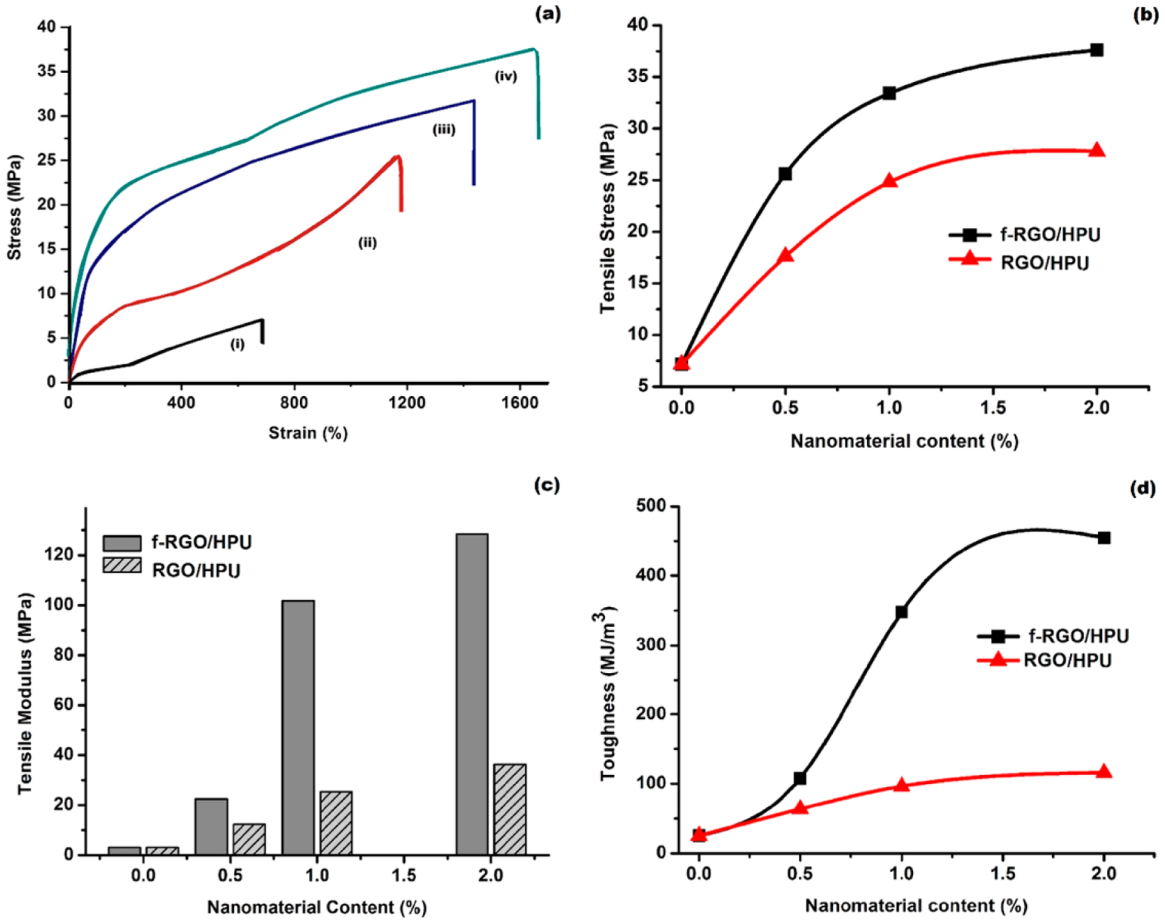

Figure 6. (a) Stress−strain profiles of (i) HPU, (ii) HPU/f-RGO0.5, (iii) HPU/f-RGO1, and (iv) HPU/f-RGO2 and (b) tensile stress, (c) tensile modulus, and (d) toughness of HPU/f-RGO and HPU/RGO nanocomposites at different weight percentages of nanomaterial.

Interestingly, elongation at break of the nanocomposites was also found to increase by more than 130% compared to pristine HPU. This is the most protuberant feature of these nanocomposites. Although the addition of graphene generally aids the enhancement of their E value, the ε% always shows complex behavior as graphene contents vary in polyurethane nanocomposites. For example, Wu et al. found a continuous decrease in ε% with an increase in the graphene content.[48] In addition, the experimental results by Chen et al. showed the nanocomposites retain an ε% almost identical to that of the pristine polyurethane.[49] In contrast, our experimental results showed an interesting and very useful mechanical behavior. A simultaneous enhancement of ε% along with improvement of σ, E, and T values was observed. Such anomalous results are due to full extension of the covalently and noncovalently bound polymer chains. Also, we presumed that polymer chains are aligned in the initial stage of tensile loading, which forces orientation of f-RGO along the loading direction. At high stress, layers of f-RGO are sliding past each other due to the presence of strong covalent bonds as well as multiple H-bonds between the f-RGO and the adjacent HPU chains. This helps to overcome the $\pi-\pi$ stacking interactions among f-RGO sheets. As f-RGO preferentially reinforced the hard segments rather than soft segments, unusual stiffness of soft segments was avoided.[45] This combined effect gives enhancement in the elongation at breaks of the nanocomposites, which has not been achieved so far. HPU/RGO nanocomposites also exhibited better elongation at break compared to pristine HPU but much less than HPU/f-RGO nanocomposites. As RGO contains few hydroxyl groups on its surface, it was incorporated in the first step of the polymerization technique. There is a chance that some of the hydroxyl groups of RGO will react with the isocyanate groups and form a few strong covalent bonds (urethane linkages).

Scheme 1. Plausible Mechanism of High Elongation and Toughness of HPU/f-RGO Nanocomposites

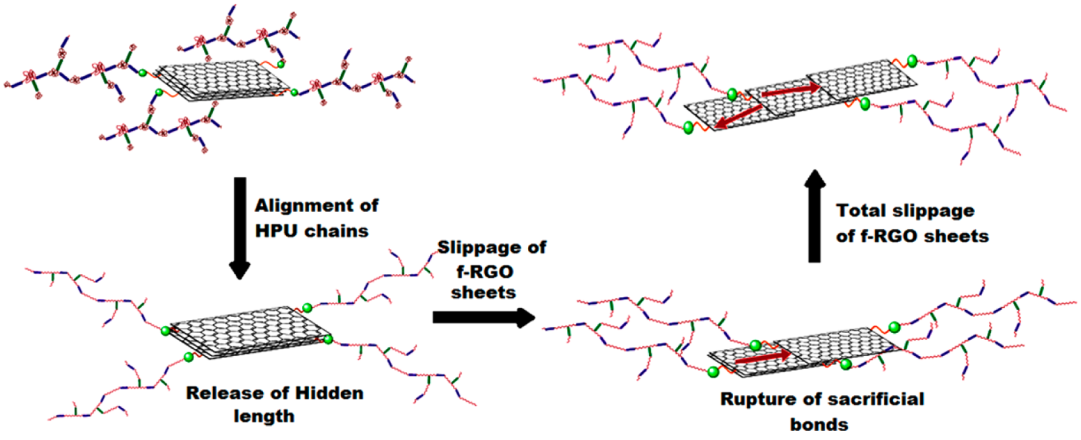

It is quite obvious that the toughness of the nanocomposite is also enhanced as it is the combined effect of strength and flexibility. To find out the reason behind such a huge enhancement in mechanical properties, we look at the toughening mechanism of biocomposites. The toughness of nanocomposites originates from secondary "sacrificial" bonds between coiled polymeric chains.[45] These sacrificial bonds are ruptured instead of the primary covalent bonds present in nanocomposites under the applied stress. This allows long hidden lengths to loosen and dissipate significant amounts of energy by maintaining structural integrity to large strains. The weak interlayer interactions of f-RGO may also be overcome without damaging the integrity of the sheet structure under the applied stress in the nanocomposites, which dissipates significant amounts of energy and thereby enhanced toughness was obtained. The H-bond interaction between hydroxyl groups of f-RGO and urethane chains mainly transferred most of the applied stress during the sliding of f-RGO layers (sacrificial bond rupture). A further increase in the applied load finally causes dissociation of these H-bonds (hidden length release). This enables the nanocomposite to enhance the inherent flexibility of the pristine HPU and to exhibit high ductility. The plausible toughening mechanism is shown in Scheme 1. Both the flexibility and ductility of nanocomposites are largely reliant on the mobility of polymer segments and f-RGO.[50] The mobility of f-RGO and polymer segments diminished as some f-RGO were bonded with HPU. This aids the load transfer between soft and hard segments. In contrast, the generation of sacrificing bonds and hidden lengths at the interfaces of nanocomposites provides an effective resolution to balance strength, toughness, and ductility. It enables one to not only control the mobility of f-RGO in the HPU matrix but also ensures efficient load transfer at the interfaces. The introduction of such biomimetic interfaces may expose a new hopeful arena for the development of high performance nanocomposites.

Thermal Properties. Nanomaterials in general influence the crystallization behavior of polyurethane. Therefore, a DSC analysis was performed in addition to a XRD study to investigate the crystallization behavior of HPU (as reported in our earlier work[6]) and HPU/f-RGO. After incorporation of 2 wt % f-RGO in HPU, T_m increased from 48.4 to 50.6 °C as shown in Figure 7. Such a small increment of T_m is due to the restriction of molecular mobility by f-RGO at the initial stage of heating. This influence depends on the interaction of f-RGO with the surrounding HPU matrix. The DSC study also demonstrated

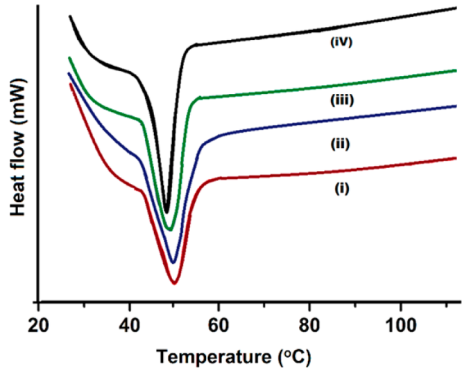

Figure 7. DSC curves of (i) HPU/f-RGO2, (ii) HPU/f-RGO1, (iii) HPU/f-RGO0.5, and (iv) HPU. [DSC curve of HPU is reproduced from our earlier work for better understanding[6]].

that the crystallization behavior was changed with loading of f-RGO as compared to HPU. The amount of crystalinity was calculated from the enthalpy data of the crystalline melting peak (Table S1, Supporting Information). This illustrates that f-RGO hasa positive effect on the crystallization process of the nanocomposite.

To verify the thermal stability of HPU (as reported in our earlier work[6]) and HPU/f-RGO, TGA was performed (Figure 8). They both exhibited a two-step degradation pattern. The degradation temperatures of HPU/f-RGO were shifted to a higher temperature compared to that of HPU. The enhanced thermostability of the nanocomposites with loading of f-RGO is due to restricted motion of the polymer chains through the different physicochemical interactions with f-RGO. Also, the improved barrier characteristics of the nanocomposite retains the generated volatiles for a longer time in the HPU matrix, which retards degradation.[39]

Electrical Property. Figure 9 depicts the electrical conductivity values of HPU and HPU/f-RGO. The variation of conductivity as a function of f-RGO content is also shown. It is observed that the conductivity increased exponentially even at low f-RGO content, followed by a slow growth at high content. The electrical conductivity jumped by almost 10 orders of magnitude from 10^{-11} to 0.16 S by incorporation of only 2 wt % of f-RGO. The formation of a conductive network in the nanocomposite is mainly influenced by the electrical conductivity.[51] The large numbers of covalent and noncovalent interactions between f-RGO and the urethane chains are due to

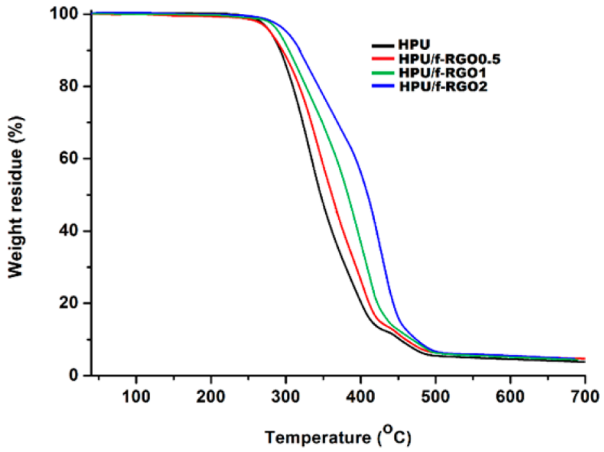

Figure 8. TGA thermograms of HPU, HPU/f-RGO0.5, HPU/f-RGO1, and HPU/f-RGO2. [TGA thermogram of HPU is reproduced from our earlier work for better understanding[6]].

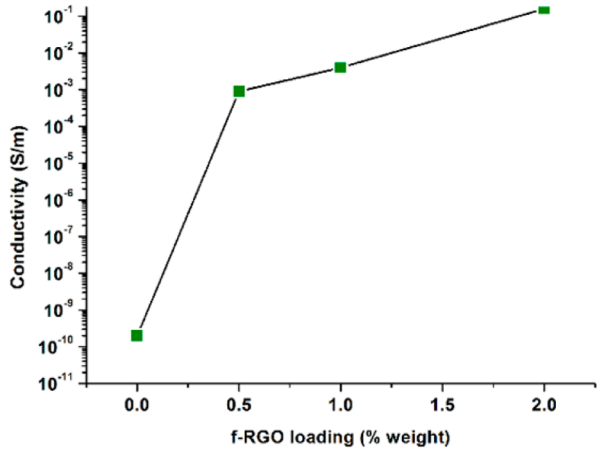

Figure 9. Electrical conductivity of HPU and its nanocomposites.

uniform distribution of f-RGO sheets in the polymer matrix. Hence, a f-RGO network is formed that helps to create conductive pathways in the nanocomposite. As a result, the electrical conductivity is enhanced in nanocomposites from pristine HPU. This electrical conductivity value is considered to be sufficient for many such practical applications.

CONCLUSIONS

The study demonstrated a new strategy to obtain an ultratough, ductile, sustainable, polymeric material. The f-RGO served as a reactive chain extender as well as nano-reinforcing material to the fabricated castor oil-based, hyperbranched, polyurethane (HPU) nanocomposite. HPU/f-RGO nanocomposites exhibited excellent mechanical properties compared to HPU/RGO nanocomposites. Also, the obtained HPU/f-RGO nanocomposites exhibited excellent electrical conductivity. This study opens the door toward RGO-based nanocomposites as superior, tough, conductive, sustainable, elastomeric materials, which have great potential in the fields of aerospace, artificial muscles, and tissue engineering.

ASSOCIATED CONTENT

Supporting Information

Images of the reaction scheme, stretchable HPU/f-RGO film, and dispersibility of f-RGO. This material is available free of charge via the Internet at http://pubs.acs.org.

AUTHOR INFORMATION

Corresponding Author

*E-mail: karakniranjan@yahoo.com. Tel: +91 3712-267327. Fax: +91 3712-267006.

Notes

The authors declare no competing financial interest.

ACKNOWLEDGMENTS

The authors express their gratitude to SAP (UGC), India,for Grant F.3-30/2009(SAP-II) and FIST program-2009 (DST), India, for Grant SR/FST/CSI-203/209/1 dated June 5, 2010. RSIC, NEHU, Shillong is gratefully acknowledged for TEM imaging. The research is funded by the Department of Science and Technology (DST), India, through the Grant SR/S3/ME/0020/2009-SERC, dated July 9, 2010.

REFERENCES

(1) Kalita, H.; Karak, N. Biobased hyperbranched shape-memory polyurethanes: Effect of different vegetable oils. *J. Appl. Polym. Sci.* **2014**, *131*, DOI: 10.1002/app.39579.

(2) Pfister, D. P.; Xia, Y.; Larock, R. C. Recent advances in vegetable oil-based polyurethanes. *Chem. Sus. Chem.* **2011**, *4*, 703−717.

(3) Xia, Y.; Larock, R. C. Vegetable oil-based polymeric materials: Synthesis, properties, and applications. *Green Chem.* **2010**, *12*, 1893−1909.

(4) Mutlu, H.; Meier, M. A. R. Castor oil as a renewable resource for the chemical industry. *Eur. J. Lipid Sci. Technol.* **2010**, *112*, 10−30.

(5) Allauddin, S.; Narayan, R.; Raju, K. V. S. N. Synthesis and properties of alkoxysilane castor oil and their polyurethane/urea−silica hybrid coating films. *ACS Sustainable Chem. Eng.* **2013**, *1* (8), 910−918.

(6) Thakur, S.; Karak, N. Castor oil-based hyperbranched polyurethanes as advanced surface coating Materials. *Prog. Org. Coat.* **2013**, *76*, 157−164.

(7) Voit, B. Hyperbranched polymers−All problems solved after 15 years of research? *J. Polym. Sci., Part A: Polym. Chem.* **2005**, *43*, 2679−2699.

(8) Mahapatra, S. S.; Yadav, S. K.; Yoo, H. J.; Cho, J. W. Highly stretchable, transparent and scalable elastomers with tunable dielectric permittivity. *J. Mater. Chem.* **2011**, *21*, 7686−7691.

(9) Kalita, H.; Karak, N. *Mesua ferrea* L. seed oil-based hyperbranched shape memory polyurethanes: Effect of multifunctional component. *Polym. Eng. Sci.* **2012**, *52*, 2454−2461.

(10) Nelson, J. K.; Fothergill, J. C. Internal charge behaviour of nanocomposites. *Nanotechnology* **2004**, *15*, 586−595.

(11) Zhu, C.; Zhai, J.; Wen, D.; Dong, S. Graphene oxide/polypyrrole nanocomposites: one-step electrochemical doping, coating and synergistic effect for energy storage. *J. Mater. Chem.* **2012**, *22*, 6300−6306.

(12) Sadu, R. B.; Chen, D. H.; Kucknoor, A. S.; Guo, Z.; Gomes, A. J. Silver-doped TiO_2/polyurethane nanocomposites for antibacterial textile coating. *BioNanoScience* **2014**, DOI: 10.1007/s12668-014-0125-x.

(13) Wei, H.; Ding, D.; Wei, S.; Guo, Z. Anticorrosive conductive polyurethane multiwalled carbon nanotube nanocomposites. *J. Mater. Chem. A* **2013**, *1*, 10805−10813.

(14) Zhu, J.; Wei, S.; Lee, I. Y.; Park, S.; Willis, J.; Haldolaarachchige, N.; Young, D. P.; Luo, Z.; Guo, Z. Silica stabilized iron particles toward anti-corrosion magnetic polyurethane nanocomposites. *RSC Adv.* **2012**, *2*, 1136−1143.

(15) Zhu, J.; Wei, S.; Haldolaarachchige, N.; Young, D. P.; Guo, Z. Electromagnetic field shielding polyurethane nanocomposites reinforced with core−shell Fe−silica nanoparticles. *J. Phys. Chem. C* **2011**, *115*, 15304−15310.
(16) Guo, Z.; Lee, S. E.; Kim, H.; Park, S.; Hahn, H. T.; Karki, A. B.; Young, D. P. Fabrication, characterization and microwave properties of polyurethane nanocomposites reinforced with iron oxide and barium titanate nanoparticles. *Acta Mater.* **2009**, *57*, 267−277.
(17) Guo, Z.; Kim, T. Y.; Lei, K.; Pereira, T.; Sugar, J. G.; Hahn, H. T. Strengthening and thermal stabilization of polyurethane nanocomposites with silicon carbide nanoparticles by a surface-initiated-polymerization approach. *Compos. Sci. Technol.* **2008**, *68*, 164−170.
(18) Guo, Z.; Park, S.; Wei, S.; Pereira, T.; Moldovan, M.; Karki, A. B.; Young, D. P.; Hahn, H. T. Flexible high-loading particle-reinforced polyurethane magnetic nanocomposite fabrication through particle-surface-initiated polymerization. *Nanotechnology* **2007**, *18*, 335704.
(19) Xu, L. Q.; Yang, W. J.; Kang, E. T.; Neoh, K. G.; Fu, G. D. Dopamine-induced reduction and functionalization of graphene oxide nanosheets. *Macromolecules* **2010**, *43*, 8336−8339.
(20) Zhu, J.; Chen, M.; He, Q.; Shao, L.; Wei, S.; Guo, Z. An overview of the engineered graphene nanostructures and nanocomposites. *RSC Adv.* **2013**, *3*, 22790−22824.
(21) Shao, L.; Quan, S.; Liu, Y.; Guo, Z.; Wang, Z. A novel "gel−sol" strategy to synthesize TiO_2 nanorod combining reduced graphene oxide composites. *Mater. Lett.* **2013**, *107*, 307−310.
(22) Shao, L.; Chang, X.; Zhang, Y.; Huang, Y.; Yao, Y.; Guo, Z. Graphene oxide cross-linked chitosan nanocomposite membrane. *Appl. Surf. Sci.* **2013**, *280*, 989−992.
(23) Zhang, X.; Alloul, O.; He, Q.; Zhu, J.; Verde, M. J.; Li, Y.; Wei, S.; Guo, Z. Strengthened magnetic epoxy nanocomposites with protruding nanoparticles on the graphene nanosheets. *Polymer* **2013**, *54*, 3594−3604.
(24) Zhu, J.; Wei, S.; Chen, M.; Gu, H.; Rapole, S. B.; Pallavkar, S.; Ho, T. C.; Hopper, J.; Guo, Z. Magnetic nanocomposites for environmental remediation. *Adv. Powder Technol.* **2013**, *24*, 459−467.
(25) Zhang, Y. H.; Han, L. F.; Xiao, Y. H.; Jia, D. Z.; Guo, Z. H.; Li, F. Understanding dopant and defect effect on H_2S sensing performances of graphene: A first-principles study. *Comput. Mater. Sci.* **2013**, *69*, 222−228.
(26) Thakur, S.; Karak, N. One-step approach to prepare magnetic iron oxide/reduced graphene oxide nanohybrid for efficient organic and inorganic pollutants removal. *Mater. Chem. Phys.* **2014**, *144*, 425−432.
(27) Zhu, J.; Wei, S.; Gu, H.; Rapole, S. B.; Wang, Q.; Luo, Z.; Haldolaarachchige, N.; Young, D. P.; Guo, Z. Understanding dopant and defect effect on H_2S sensing performances of graphene: A first-principles study. *Environ. Sci. Technol.* **2012**, *46*, 977−985.
(28) Zhu, J.; Wei, S.; Haldolaarachchige, N.; He, J.; Young, D. P.; Guo, Z. Very large magnetoresistive graphene disk with negative permittivity. *Nanoscale* **2012**, *4*, 152−156.
(29) Zhu, J.; Luo, Z.; Wu, S.; Haldolaarachchige, N.; Young, D. P.; Wei, S.; Guo, Z. Magnetic graphene nanocomposites: Electron conduction, giant magnetoresistance and tunable negative permittivity. *J. Mater. Chem.* **2012**, *22*, 835−844.
(30) Zhu, J.; Chen, M.; Qu, H.; Zhang, X.; Wei, H.; Luo, Z.; Colorado, H. A.; Wei, S.; Guo, Z. Interfacial polymerized polyaniline/graphite oxide nanocomposites toward electrochemical energy storage. *Polymer* **2012**, *53*, 5953−5964.
(31) Zhu, J.; Gu, H.; Luo, H.; Haldolaarachige, N.; Young, D. P.; Wei, S.; Guo, Z. Carbon nanostructure-derived polyaniline metacomposites: Electrical, dielectric, and giant magnetoresistive properties. *Langmuir* **2012**, *28*, 10246−10255.
(32) Zhu, J.; Zhang, X.; Haldolaarachchige, N.; Wang, Q.; Luo, Z.; Ryu, J.; Young, D. P.; Wei, S.; Guo, Z. Polypyrrole metacomposites with different carbon nanostructures. *J. Mater. Chem.* **2012**, *22*, 4996−5005.
(33) Li, Y.; Zhu, J.; Wei, S.; Ryu, J.; Wang, Q.; Sun, L.; Guo, Z. Poly(propylene) nanocomposites containing various carbon nanostructures. *Macromol. Chem. Phys.* **2011**, *212*, 2429−2438.
(34) Li, Y.; Zhu, J.; Wei, S.; Ryu, J.; Sun, L.; Guo, Z. Poly(propylene)/graphene nanoplatelet nanocomposites: melt rheological behavior and thermal, electrical, and electronic properties. *Macromol. Chem. Phys.* **2011**, *212*, 1951−1959.
(35) Tien, H. W.; Huang, Y. L.; Yang, S. Y.; Hsiao, S. T.; Wang, J. Y.; Chi, C.; Ma, M. Graphene nanosheets deposited on polyurethane films by self-assembly for preparing transparent, conductive films. *J. Mater. Chem.* **2011**, *21*, 14876−14883.
(36) Jung, Y. C.; Kim, J. H.; Hayashi, T.; Kim, Y. A.; Endo, M.; Terrones, M.; Dresselhaus, M. S. Fabrication of transparent, tough, and conductive shape-memory polyurethane films by incorporating a small amount of high-quality graphene. *Macromol. Rapid Commun.* **2012**, *23*, 628−634.
(37) Park, J.; Yan, M. Covalent functionalization of graphene with reactive intermediates. *Acc. Chem. Res.* **2013**, *46*, 181−189.
(38) Thakur, S.; Karak, N. Bio-based tough hyperbranched polyurethane−graphene oxide nanocomposites as advanced shape memory materials. *RSC Adv.* **2013**, *3*, 9476−9482.
(39) Compton, O. C.; Cranford, S. W.; Putz, K. W.; An, Z.; Brinson, L. C.; Buehler, M. J.; Nguyen, S. T. Tuning the mechanical properties of graphene oxide paper and its associated polymer nanocomposites by controlling cooperative intersheet hydrogen bonding. *ACS Nano* **2012**, *6*, 2008−2019.
(40) Wang, X.; Hu, Y.; Song, L.; Yang, H.; Xing, W.; Lu, H. In situ polymerization of graphene nanosheets and polyurethane with enhanced mechanical and thermal properties. *J. Mater. Chem.* **2011**, *21*, 4222−4227.
(41) Thakur, S.; Karak, N. Green reduction of graphene oxide by aqueous phytoextracts. *Carbon* **2012**, *50*, 5331−5339.
(42) Thakur, S.; Das, G.; Raul, P. K.; Karak, N. Green one-step approach to prepare sulfur/ reduced graphene oxide nanohybrid for effective mercury ions removal. *J. Phys. Chem. C* **2013**, *117* (15), 7636−7642.
(43) Karak, N.; Rana, S.; Cho, J. W. Synthesis and characterization of castor oil modified hyperbranched polyurethanes. *J. Appl. Polym. Sci.* **2009**, *112*, 736−743.
(44) Zhu, J.; Wei, S.; Ryu, J.; Budhathoki, M.; Liang, G.; Guo, Z. In situ stabilized carbon nanofiber (CNF) reinforced epoxy nanocomposites. *J. Mater. Chem.* **2010**, *20*, 4937−4948.
(45) Pei, A.; Malho, J. M.; Ruokolainen, J.; Zhou, Q.; Berglund, L. A. Strong nanocomposite reinforcement effects in polyurethane elastomer with low volume fraction of cellulose nanocrystals. *Macromolecules* **2011**, *44*, 4422−4427.
(46) Chen, D.; Zhu, H.; Liu, T. In situ thermal preparation of polyimide nanocomposite films containing functionalized graphene sheets. *ACS Appl. Mater. Interfaces* **2010**, *2*, 3702−3708.
(47) Park, O. K.; Hwang, J. Y.; Goh, M.; Lee, J. H.; Ku, B. C. Mechanically strong and multifunctional polyimide nanocomposites using amimophenyl functionalized graphene nanosheets. *Macromolecules* **2013**, *46*, 3505−3511.
(48) Wu, C.; Huang, X.; Wang, G.; Wu, X.; Yang, K.; Li, h.; Jiang, P. Hyperbranched-polymer functionalization of graphene sheets for enhanced mechanical and dielectric properties of polyurethane composites. *J. Mater. Chem.* **2012**, *22*, 7010−7019.
(49) Chen, Z.; Lu, H. Constructing sacrificial bonds and hidden lengths for ductile graphene/polyurethane elastomers with improved strength and toughness. *J. Mater. Chem.* **2012**, *22*, 12479−12490.
(50) Khan, U.; May, P.; O'Neill, A.; Coleman, J. N. Development of stiff, strong, yet tough composites by the addition of solvent exfoliated graphene to polyurethane. *Carbon* **2010**, *48*, 4035−4041.
(51) Raghu, A. V.; Lee, Y. R.; Jeong, H. M.; Shin, C. M. Preparation and physical properties of waterborne polyurethane/functionalized graphene sheet nanocomposites. *Macromol. Chem. Phys.* **2008**, *209*, 2487−2493.